Automotive Experiences
Vol. 9 No. 2 (2026) pp. 345-364
p-ISSN: 2615-6202 e-ISSN: 2615-6636

Research Paper

The Effect of Curvature on the Thermal-Hydraulic Performance of Serpentine Battery Cooling Channels

Teguh Hady Ariwibowo[1], **Lucky Pradigta Setiya Raharja**[2], **Satworo Adiwidodo**[3], **Fengky Adie Perdana**[3], **Nila Alia**[3], **Burniadi Moballa**[4], **Muh. Anis Mustaghfirin**[4], **Arya Rafi Abrari**[5], **Muhammad Aghist Fitrony**[6], **Charitsma Tsani**[1], **Probo Yekti Salsabilla Adelwise**[1], **Putri Dwi Imandini**[1]

[1]Department of Power Plant Engineering, Electronic Engineering Polytechnic Institute of Surabaya, Surabaya 60111, Indonesia
[2]Department of Electrical Engineering, Electronic Engineering Polytechnic Institute of Surabaya, Surabaya 60111, Indonesia
[3]Department of Mechanical Engineering, State Politechnic of Malang, Malang 65145, Indonesia
[4]Department of Marine Engineering, Shipbuilding Institute of Polytechnic Surabaya, Surabaya 60111, Indonesia
[5]PT. Guntner Indonesia, Pasuruan 67154, Indonesia
[6]Department of Mechanical Engineering, Pohang University of Science and Technology, Republic of Korea

teguhhady@pens.ac.id

https://doi.org/10.31603/ae.15222

Published by Automotive Laboratory of Universitas Muhammadiyah Magelang

Article Info
Submitted: 06/11/2025
Revised: 25/05/2026
Accepted: 28/05/2026
Online first: 12/06/2026

Abstract

Efficient battery thermal management systems (BTMS) are essential for ensuring the safety and performance of lithium-ion batteries in electric vehicles. This study numerically investigates the influence of serpentine channel curvature on the thermal and hydraulic characteristics of a liquid-cooled prismatic battery module. Four channel designs were evaluated: a base case and three serpentine configurations with curvature values of 0.075 mm^{-1}, 0.1 mm^{-1}, and 0.15 mm^{-1}. Simulations were conducted under steady-state and transient conditions with discharge rates of 0.5 to 2 C and mass flow rates of 2.41×10^{-3} to 3.61×10^{-2} kg/s. The results show that higher curvature and mass flow rates reduce maximum battery temperature and improve temperature uniformity, but at the expense of increased pressure drop and pumping power. At 3.61×10^{-2} kg/s, the base-case channel exhibited a 28% increase in pressure drop compared to 2.41×10^{-2} kg/s, while the 0.15 mm^{-1} channel recorded up to a 60% rise under the same condition. Transient analysis revealed that curved channels enhanced heat dissipation, achieving up to 8.56% higher cooling performance than the base case. These findings highlight the trade-off between thermal improvement and hydraulic penalty, providing valuable guidance for optimizing liquid-cooled BTMS in electric vehicle applications.

Keywords: Battery thermal management; Serpentine channel; Numerical simulation

1. Introduction

Global effort to mitigate climate change and achieve net-zero emissions by 2050 necessitate a profound energy transition, particularly within the transportation sector, which represents one of the largest contributors to greenhouse gas emissions [1], [2]. Consequently, the advancement and widespread adoption of Electric Vehicles (EVs) have become a strategic pathway to reduce emissions and decrease reliance on fossil fuels [3]. This transition toward electric mobility is significant not only for environmental protection but also for ensuring the sustainability of modern urban ecosystems. However, the effectiveness of this transformation depends heavily on the maturity and reliability of its core enabling technology: the battery system [4].

Lithium-ion batteries (LIBs) currently dominate the market due to their high energy density, long cycle life, and overall efficiency [5], [6] Despite these advantages, LIBs generate considerable heat during charging and discharging, particularly under fast charging conditions [7]. This excessive heat can induce hot spots, accelerate component degradation, and even cause irreversible damage. Therefore, an efficient thermal management system is essential to ensure reliable performance [8], [9].

The Thermal Management System (BTMS) is essential for regulating temperature and ensuring the safe and reliable operation of batteries [10]. Among the available strategies, liquid cooling systems are widely regarded as effective and practical solutions for modern EV applications. In particular, indirect liquid cooling, where the coolant circulates through a cold plate, has become a primary focus for the industry due to its balance of efficiency and safety [11]. The performance of this method depends heavily on the cold plate design.

The design of cooling plates, particularly their channel configuration, is fundamental to maximizing heat transfer. While previous studies have shown that straight channel designs exhibit suboptimal efficiency [12], prompting increased interest in more advanced geometries, serpentine channel designs demonstrate superior performance by enhancing flow turbulence and improving heat dissipation [13]. Several studies, including those by Huo *et al*. [14] and Monika *et al*. [15], have highlight the influence of channel design parameters such as channel diameter, length, shape, and number on the system's overall thermal performance. However, the effect of curvature in serpentine channels remains underexamined in the literature [16].

The primary advantage of curved channels is their ability to harness centrifugal forces [17]. As fluid flows through the bends, these forces drive the fluid across the channel cross-section, generating dean vortices. This phenomenon drastically enhances thermal mixing by disturbing the thermal boundary layer along the channel walls, the results in a more uniform temperature distribution and a higher heat transfer coefficient [13]. The strength of this curvature effect has been proven effective in various engineering fields, such as heat exchangers [18], microfluidics [19], particle filtration [20], and biomedical applications [21]. In the biomedical field, studies have fundamentally demonstrated that high curvature, with a curvature height (Hc) of 0.05mm, significantly alters fluid flow patterns by generating strong dean vortices with De=1.033 [22].

Although previous studies have contributed valuable insights into serpentine channel design for battery thermal management, several important gaps remain. For instance, Monika and Datta [22] compared different channel designs under steady-state conditions but did not explore how curvature affects the flow behaviour. Fan *et al.* [23] proposed a new secondary flow serpentine plate and reported improved cooling performance, yet their work focused on a fixed curvature without systematically varying it. Similarly, Qian *et al*. [24] examined mini-channel cooling for lithium-ion batteries, but their analysis was limited to transient thermal response under constant curvatures.

What makes our study different from these earlier works is that we specifically focus on curvature as a design variable. While curvature is known to generate Dean vortices and enhance heat transfer in other engineering fields such as heat exchangers and microfluidics [18], [19], [20], [21], its role in serpentine cooling channels for battery applications has received very little attention. To the best of our knowledge, no previous study has systematically varied curvature (0.075 mm^{-1}, 0.1 mm^{-1}, and 0.15 mm^{-1}) and evaluated its effects under both steady-state and transient discharge conditions.

Therefore, the main scientific contribution of this work is threefold. First, we provide a quantitative understanding of how curvature affects not only the maximum battery temperature and temperature uniformity but also the pressure drop and pumping power. Second, we compare the thermal performance of curved channels against a conventional straight-serpentine base case across a range of mass flow rates (2.41×10^{-3} to 3.61×10^{-2} kg/s) and discharge rates (0.5 to 2C). Third, we include a transient analysis up to 3600 seconds, which reveals how curvature influences the time needed to reach thermal equilibrium and the heat dissipation rate during the early discharge period. Together, these elements allow us to evaluate the trade-off between cooling improvement and hydraulic penalty, which is essential for practical BTMS design.

By clarifying these aspects, we believe our study fills an important gap and offers useful guidance for engineers who need to choose an appropriate channel curvature for liquid-cooled battery packs in electric bikes.

2. Methods

The proposed cooling thermal performance is examined under various discharging processes, including an extreme condition of 2 C. It is important to note that this rate exceeds the manufacturer specified maximum continuous discharge of 1.0 C written in **Table 1** specifically to investigate the system thermal limits. C rate is a measure of rate at which a battery is charged/discharged relative to its maximum capacity [25]. A discharge current of 20 A is applied at 1 C rate, while 40 A is applied at 2 C rate.

2.1. *Numerical Model*

The schematic design of the thermal management system features 24 prismatic ABC LFP 20Ah cells manufactured Indonesian battery company known as PT Intercallin shown in **Figure 1**. The cells are connected in a series configuration which forms a battery pack with a total capacity of 1.53 kWh, suitable for electric bike applications. The dimensions of each prismatic cell are 143.3 mm in height, 65.2 mm in width, and 22.5 mm in thickness, as illustrated in **Figure 1b**. The specifications of the battery are shown in **Table 1**.

The proposed cooling solution involves two cooling plates with serpentine channel attached to the battery surface. Four different cooling plate designs were examined to assess their impact on the battery thermal performance. Coolant was chosen as the working fluid due to its low viscosity and high thermal conductivity [26] and

Table 1. ABC LFP 20Ah battery datasheet

Item	General Parameter	Remark
Rated capacity	Standard 21 Ah Minimum 20 Ah	0.2 C at 20±5 °C
Nominal voltage	3.2V	Operating voltage
Discharge current	Standard: 0.2 C Fast: 0.5 C Max: 1.0 C	For specific value should be determined according to the combination structure (series and parallel), and the maximum operating current is set at temperature condition not exceeding 60 °C. *For maximum continuous discharge current, only for single cell
Internal Resistenace	4.3 mΩ	-
Weight	430 ± 5 g	-
Cycle characteristic	≥2000 times (100% DOD)	The residual capacity is not less than 80% of rated capacity at 0.2 C rate.

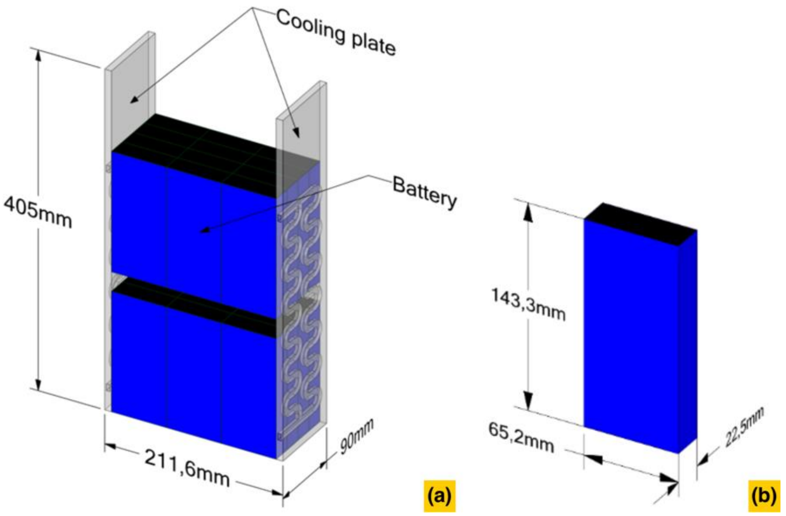

Figure 1. Schematic of: (a) Overall view of battery pack; (b) Dimensions of a single battery cell

aluminum was selected as the heat sink material. The battery cell has thermal conductivity varies in-plane and cross-plane directions with the specific values listed in **Table 2** [27], [28], [29].

Figure 2 illustrates the different geometries of the cooling plate channel investigated. A 'Base case' with a simple channel design was used as a reference. Based on this design, three designvariations were created based on channel curvature, with values of 0.075 mm⁻¹, 0.1 mm⁻¹, and 0.15 mm⁻¹, respectively. Curvature is an inverse of radius (r).

2.2. Governing Equations

The governing equations related to the battery and coolant are described here. The equations governing the fluid region consist of the conservation of mass (Eq. (1)), momentum (Eq. (2)), and energy (Eq. (3)) [15]:

$$\nabla \cdot \vec{v} = 0 \tag{1}$$

$$\rho_l[(\vec{v} \cdot \nabla)\vec{v}] = -\nabla P + \mu_l \nabla^2 \vec{v} \tag{2}$$

$$\rho_l c_{p,l} \frac{\partial T_l}{\partial t} + \nabla \cdot (\rho_l c_{p,l} \vec{v} T_l) = \nabla \cdot (k_l \nabla T_l) \tag{3}$$

where, v and ρ_l represent the flow rate and density of liquid, respectively. $\mu_l, c_{p,l}$, and T_l denote the kinetic viscosity, specific heat capacity, and temperature of liquid, in that order. Furthermore, k_l is the thermal conductivity of liquid.

The equation for the energy conservation within the solid region of the liquid-cooled plate is following Eq. (4).

$$\frac{\partial}{\partial t}(\rho_s \cdot C_{p,s} \cdot T_s) = \nabla \cdot (k_s \cdot \nabla T_s) \tag{4}$$

where, $\rho_s, C_{p,s}$ and T_s represents the solid region density, heat capacity, and temperature of the solid region. k_s is the thermal conductivity of the solid.

Energy balance for the batteries is expressed by Eq. (5) [30].

$$\rho C_p \left[\frac{\partial T}{\partial t} + \nabla.(\vec{u}\,T)\right] = k\nabla^2 T + Q_{gen} \tag{5}$$

The flow rate is determined by the Reynolds number (Re). Given that minichannel flows typically have low Re values [23], [31], this research utilizes Re variations from 100 to 1500. Since the Re values are all below 2300, a laminar flow model is applied in the simulation. Eq. (6) and Eq. (7) are used to calculate Re and D_h.

$$D_h = \frac{4A_c}{P} \tag{6}$$

$$Re = \frac{\rho \cdot v \cdot D_h}{\mu} \tag{7}$$

where D_h is the hydraulic diameter of coolant flow, A_c is cross sectional surface area and P is wetted perimeter.

The pressure drop across the cooling plate is given by Eq. (8) [32]:

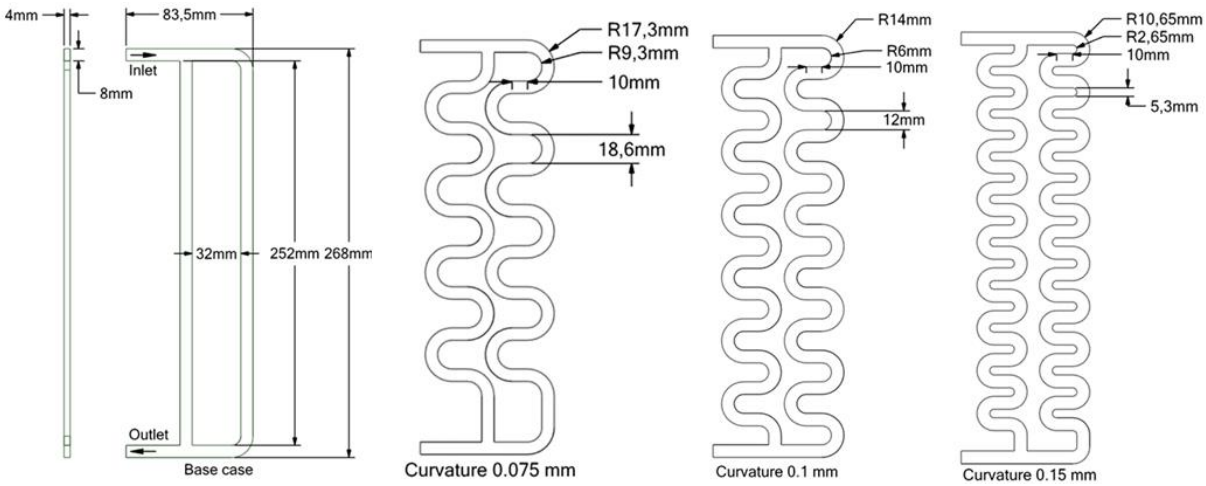

Figure 2. Geometry variations

$$\Delta P = -\int_{p1}^{p2} dp = f\frac{\rho u_m^2}{2D}\int_{x1}^{x2} dx = f\frac{\rho u_m^2}{2D}(x_2 - x_1) \tag{8}$$

Table 2. Thermophysical properties of battery, coolant, and aluminium

Name	Density (kg/m³)	Specific heat capacity (J/kg·K)	Thermal conductivity (W/m·K)	Viscosity (kg/m·s)
Battery cell	2277.96	1181.3	$K_{\parallel}$=21.5, $k_{\perp}$=0.76	-
Coolant [33]	1074.7	3419.4	0.36	0.00402
Aluminium [34]	2719	871	202.4	-

where, u_m is the mean fluid velocity over the cube cross section, calculated using the Eq. (9).

$$u_m = \frac{\dot{V}}{\rho.A} \tag{9}$$

The energy conservation equation is required to determine the heat dissipation. Considering the battery as the system, the energy conservation equation can be formulated as following Eq. (10).

$$\frac{dE_{cv}}{dt} = \dot{Q} - \dot{W} \tag{10}$$

where $\dot{Q}$ is the heat dissipated from the battery to the cooling fluid in watts (W), and $\dot{W}$ is the power produced by the battery, also in watts (W). Assuming steady state conditions, the equation can be expressed as following Eq. (11).

$$\dot{Q} = \dot{W} \tag{11}$$

2.3. *Heat Generation Model and Limitations*

Battery heat generation (Q_{gen}) during charging and discharging comes from two sources that are irreversible heat and reversible heat which can be written as Eq. (12) [35], [36].

$$Q_{gen} = Q_{irr} + Q_{rev} = I(V_{oc} - V_{battery}) - IT\frac{dV_{oc}}{dT} \tag{12}$$

where Q_{irr} is the irreversible heat and Q_{rev} is the reversible heat. $I, V_{oc}, V_{battery}$ and $\frac{dV_{oc}}{dT}$ are the current, open circuit voltage, battery voltage, and entropy coefficient, respectively.

In this study, the open-circuit voltage is considered to be the same as the battery's maximum voltage. Additionally, the entropy coefficient is not included in calculations, as its impact is considered insignificant based on previous research [37]. Therefore, the Eq. (13) can be simplified as [38], [39]:

$$Q_{gen} = \frac{I^2 \cdot R_{battery}}{V_{battery}} \tag{13}$$

where $R_{battery}$ is the battery internal resistance and $V_{battery}$ is the volume of battery.

The heat generation model used in this paper has several key limitations. First, the model ignores the reversible (entropic) heat term, assuming it contributes less than 2% at a 1 C discharge rate. But at lower rates (below 0.5 C), reversible heat can actually dominate, so the model's accuracy drops [40]. Second, internal resistance is treated as constant, even though it changes with temperature, state of charge (SOC), and battery aging [41]. That means the model can't capture the extra heat produced at low temperatures or how heat generation changes over the battery's life. Third, heat generation is assumed to be uniform across the whole battery kernel, ignoring local hot spots near terminals or current collectors that happen when current distribution isn't even. Fourth, even though thermal conductivity is modeled as anisotropic, the material's thermal properties are still assumed to be constant with temperature [42].

2.4. *Data Reduction*

The purpose of creating an effective Battery Thermal Management System (BTMS) is to maintain battery cells within optimal temperature range and ensure battery temperature uniformity across the battery module. To evaluate how well a BTMS performance is, two key metrics are used: maximum battery temperature ($T_b max$) and battery temperature difference (ΔT_b) can be calculated as Eq. (14).

$$\Delta T_b = T_b max - T_b min \tag{14}$$

where $T_b min$ is the minimum battery temperature.

In liquid-cooled BTMS, the thermal behaviour of the battery involves a trade-off between the heat transfer efficiency and the pressure drop characteristics of the coolant flow inside the cold plates. To assess the overall performance of the cold plates, considering both thermal and hydraulic aspects, a dimensionless parameter j is employed [43]. The dimensionless parameter j, cooling efficiency coefficient, is derived from the ratio of heat dissipated to the pumping power which written as follows Eq. (15) to Eq. (17) [23].

$$\dot{Q}_{dis} = \dot{m} \cdot c_p \cdot (T_{in} - T_{out}) \tag{15}$$

$$P_{pump} = \Delta P \cdot V_{in} = (P_{in} - P_{out}) \cdot A_{in} \cdot v_{in} \quad (16)$$

$$j = \frac{Q_{dis}}{P_{pump}} \quad (17)$$

where $\dot{Q}_{dis}$ is the heat dissipated by cold plate, $\dot{m}$ is the mass flow rate (kg/s), P_{pump} is the pumping power (W), ΔP is the pressure drop of coolant flow (Pa) and V_{in} is the volume flow rate at the inlet (L/min). P_{in}, P_{out}, A_{in} and v_{in} represent the pressure inlet (Pa), pressure outlet (Pa), inlet channel area (m^2) and inlet channel velocity (m/s).

Dean number is utilized to understand curvature phenomena on the circuit. The dean number is written as follow Eq. (18).

$$De = Re\sqrt{\frac{D_h}{2R_c}} \quad (18)$$

2.5. *Numerical Setup*

The governing equations were solved using a commercial CFD software with a pressure-based solver, employing second-order upwind discretization for all equations and the SIMPLE method for pressure-velocity coupling. Under-relaxation factors of 0.3, 0.7, and 1 were applied to the pressure, momentum, and energy equations, respectively. Convergence criteria for mass and momentum were set at 10^{-3}, and for energy at 10^{-6}.

2.6. *Boundary Conditions*

Both steady state and transient analysis are performed. The system's initial temperature was set to 25 °C, and simulations were performed with a time step size of 5 seconds. For all simulations, the fluid inlet temperature was fixed at 20 °C, and a pressure outlet boundary condition was applied at the outlet. The walls were set into adiabatic. The battery was set as the heat source. Battery discharge rates of 0.5, 1, and 2 C were examined. The steady-state analysis examined five variations of the mass flow rate whereas the transient analysis considered three variations as shown in Table 3. These three transient cases were selected to represent low, medium, and high mass flow rate conditions.

Although the battery's maximum rated specification is only 1 C, we tested our cooling plate all the way up to 2 C. This was done to account for possible extreme conditions in the field and to make sure the battery stays safe. In line with that, we ran transient simulations at 0.5, 1, and 2 C to see how the temperature responds under harsh situations. Steady-state simulations were kept between 0.5 C and 2 C because we wanted to focus on how curvature and flow rate affect performance.

2.7. *Grid Independence*

Five grids were used to conduct the grid independence test; 740,398 (extra coarse); 1,282,381 (coarse); 2,322,094 (medium); 5,474,822 (fine) and 28,392,381 (extra fine). Combination of tetrahedral and hexahedral mesh was applied for the numerical model as shown in Figure 3a and Figure 3b. For all mesh, the battery is subjected to a discharge rate of 1 C, and the inlet flow temperature is at 20 °C. The deviation between the maximum battery temperature of the fine and extra fine mesh is 0.13% as shown in Figure 3c. Therefore, a grid number of 5,474,822 was chosen.

3. Verification, Results and Discussion

This section describes the steady state and transient solutions obtained for the battery pack model including the base case and curvature cooling channels. Battery temperature distribution, maximum battery temperature ($T_b max$), battery temperature difference (ΔT_b) and heat dissipation rate under different mass flow rates and discharge rates are presented. Variations in curvature can result in different flow characteristics. Furthermore, a transient analysis is conducted as well to observe time dependent variables similar to steady state condition. A total time of 3600s was performed.

3.1. *Verification*

The accuracy of the governing equations and the modelling of battery temperature is confirmed using empirical research [34]. In that prior research,

Table 3. Boundary conditions

Analysis	Discharge rate	Current (A)	Mass flow rate (kg/s)
Steady	0.5 C	10	0.002412
	1 C	20	0.007236
	2 C	40	0.01206
			0.021708
			0.03618
Transient	0.5 C	10	0.002412
	0.5 C	10	0.01206
	1 C	20	0.03618

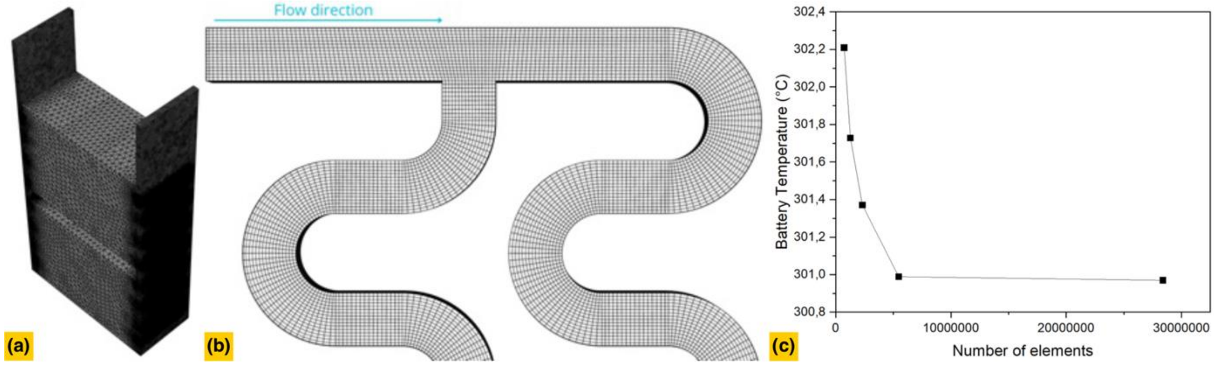

Figure 3. (a) Overall mesh view; (b) Detailed flow mesh view; (c) Grid independence test

various discharge experiments were conducted on a battery cell without BTMS, measuring the battery temperature. To verify the current method, a model of a battery cell was developed using the equations described earlier.

Figure 4 displays the predicted results from the current work alongside the experimental results [34]. The experiments used five T-type thermocouples under a constant temperature of 30 °C. The numerical results for the battery temperature variation closely match the experimental data at 3 C discharge rate. This confirms the reliability of both the heat generation equation and the numerical method used in this study with a maximum deviation of 2.35%. **Figure 4b** shows the verification of the flow pressure drop based on the Darcy-Weisbach equation and the Poiseuille number. The maximum pressure drop deviation reaches 7.78%. This indicates that the simulation data to be used is quite reliable.

3.2. *Effect of Curvature*

Previous studies have studied the effect of mass flow rate of coolant flow in reducing maximum temperature and temperature difference in battery. Monika and Datta [22] reports that both parameters reduced as the mass flow rate ($\dot{m}$) increases in several cooling channel designs. Same result was found by Fan *et al.* [23] as they performed a numerical simulation of various secondary flow serpentine cooling channel for BTMS. However, these studies did not specifically explore the role of curvature in serpentine channels, even though curvature can create strong secondary flows that help improve heat transfer [44]. Therefore, we investigate how the curvature of serpentine cooling channels affects thermal performance. The results from our numerical simulations are shown in **Figure 5**.

The performance of lithium-ion batteries (LIBs) is highly influenced by their operating temperature, with the optimal range typically between 20 °C to 40 °C [45], [46]. **Figure 5** shows how curvature affects the maximum battery temperature ($T_b max$) and battery temperature difference (ΔT_b). Generally, both figures show a similar trend, with a sharp decline from the first to the second mass flow rate. In **Figure 5a** the $T_b max$

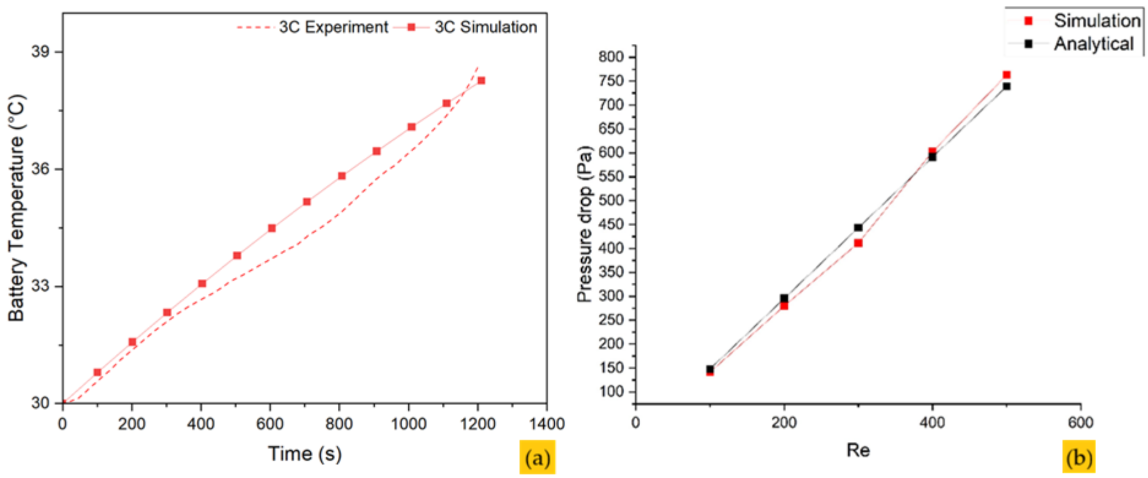

Figure 4. Verification of (a) temperature (b) pressure drop [34]

shows a gradual decrease as the mass flow rate increases, which is consistent with results obtained in previous studies [47], [48]. These phenomena is a result of Eq. (15) showing that increasing the mass flow rate enhances the heat transfer rate ($\dot{Q}_{dis}$), which in turn lowers the battery's maximum temperature.

During the first increase in mass flow rate, all cooling channel variations show a sharp decline in $T_b max$ as can be seen in **Figure 5a**. For instance, in the 0.15mm^{-1} curvature cooling channel at 2 C discharge rate, $T_b max$ declined by as much as 16.93% as the mass flow rate go up from 2.41 × 10^{-3} kg/s to 7.23×10^{-3} kg/s. As the mass flow rate increases, the $T_b max$ value shows minimal change, indicated by the gradual trend of $T_b max$ after the mass flow rate exceeds 7.23×10^{-3} kg/s. The results indicate that the serpentine cooling channel performs better at low mass flow rates, which aligns with findings from previous studies [49]. In addition, the difference in $T_b max$ between the base-case configuration and the three curvature variations becomes more noticeable at higher mass flow rates, as shown by the widening gap between their value in $T_b max$.

One of the most critical aspects of a Battery Thermal Management System (BTMS) is maintaining a temperature difference within the battery below 5 °C [50]. Temperature non-uniformity can shorten battery lifespan and lead to poor performance [51]. As shown in **Figure 5b**, the ΔT_b values at 0.5 C and 1 C discharge rates remain below 5 °C which still within the acceptable temperature difference range. However, this is not the case for the 2 C discharge rate. Although the $T_b max$ at 2 C does not exceed the allowable operating temperature, the ΔT_b surpasses 5 °C, reaching a maximum of 14.5 °C at the lowest mass flow rate. This high temperature difference occurs because batteries next to the cooling plate maintain lower temperatures, whereas batteries surrounded by other cells has higher temperature as can be seen in **Figure 6**. Therefore, the central batteries have difficulty in dissipating heat effectively which causes temperature gradient.

The heat dissipation rate is defined in Eq. (15), and the results of this study are presented in **Figure 7**. As shown in **Figure 7**, the heat dissipation rate for all cooling channel variations remains constant as the mass flow rate increases. In this study, the curvature pattern does not have much impact on the heat transfer rate. This may be due to the simulation assumption used is steady state which refers to infinite time until steady state. The steady state of each case may be different depending on the flow rate produced. So, in this study it is necessary to look at the transient condition aspect.

Additionally, Notable differences in heat dissipation are observed only with varying C-rates. An increase in C-rate leads to higher heat dissipation due to increased heat generation. According to Eq. (7), heat generation is directly proportional to the current; therefore, higher C-rates result in greater heat generation and, consequently, greater heat dissipation. The maximum heat dissipation is calculated to be 165.12 W at a C-rate of 2C, while the minimum is 10.32 W at a C-rate of 0.5C.

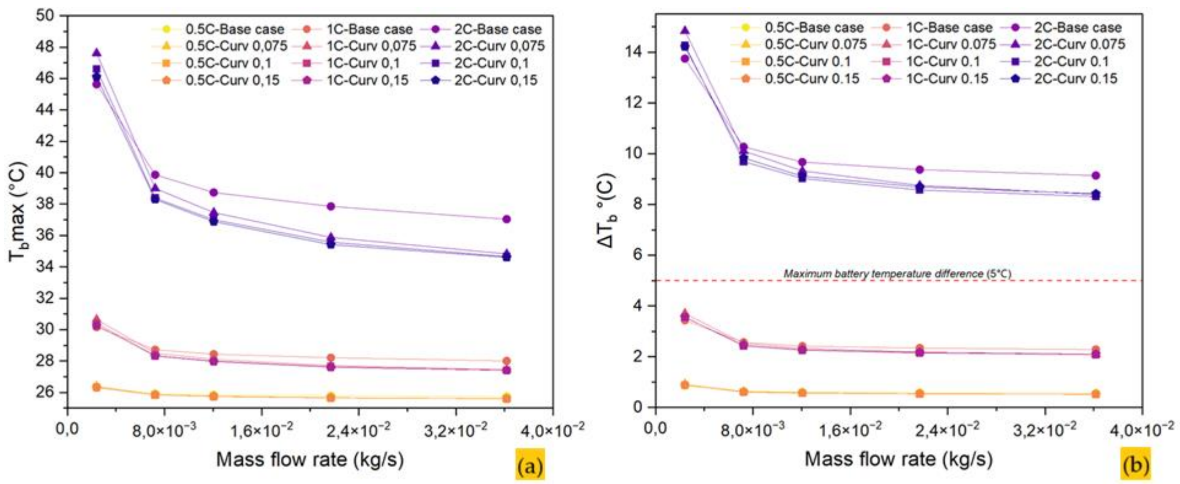

Figure 5. Curvature effect on: (a) Maximum battery temperature ($T_b$max); (b) Battery temperature difference (ΔT_b)

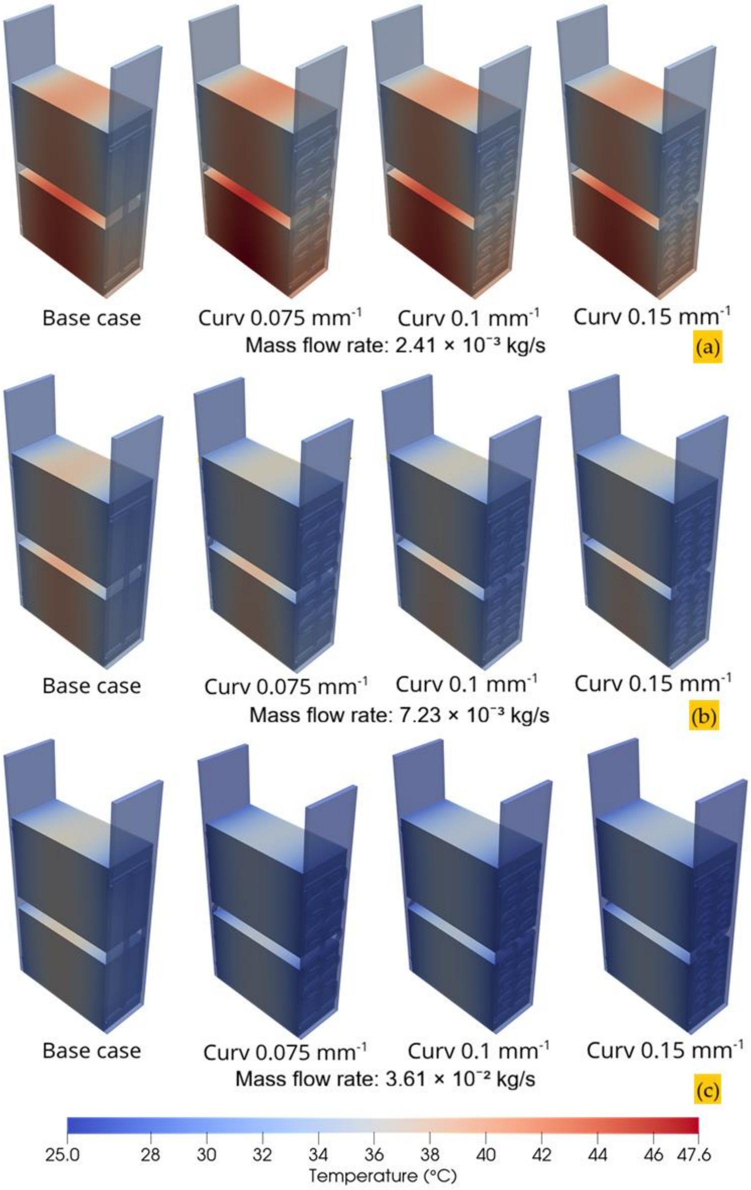

Figure 6. Battery temperature distribution of various variations at 2 C discharge rate: (a) Mass flow rate: 2.41×10^{-3} kg/s; (b) Mass flow rate: 7.23×10^{-3} kg/s; (c) Mass flow rate: 3.61×10^{-2} kg/s.

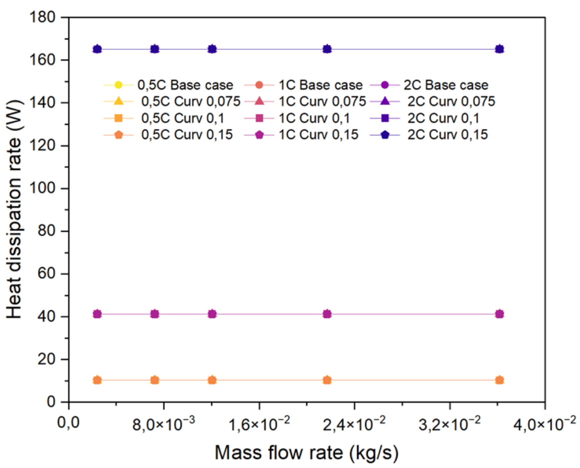

Figure 7. Heat dissipation rate of different variations and discharge rates

3.3. Flow Analysis

As shown in Figure 8a, curvature has a significant influence on the pressure drop in the channel. A sharper curvature results in a higher pressure drop, thereby increasing the required pumping power as shown in Figure 8b. At a high mass flow rate of 3.61×10^{-2} kg/s, the increase in pressure drop is notably sharp, approximately 28% for the base case channel compared to the low mass flow rate of 2.41×10^{-2} kg/s. In contrast, for a channel with a sharp curvature of 0.15 mm^{-1}, the pressure drop increases by up to 60% at the same mass flow rate. This difference is attributed to the increase in radial flow velocity, which generates a stronger centrifugal force. This force induces a more

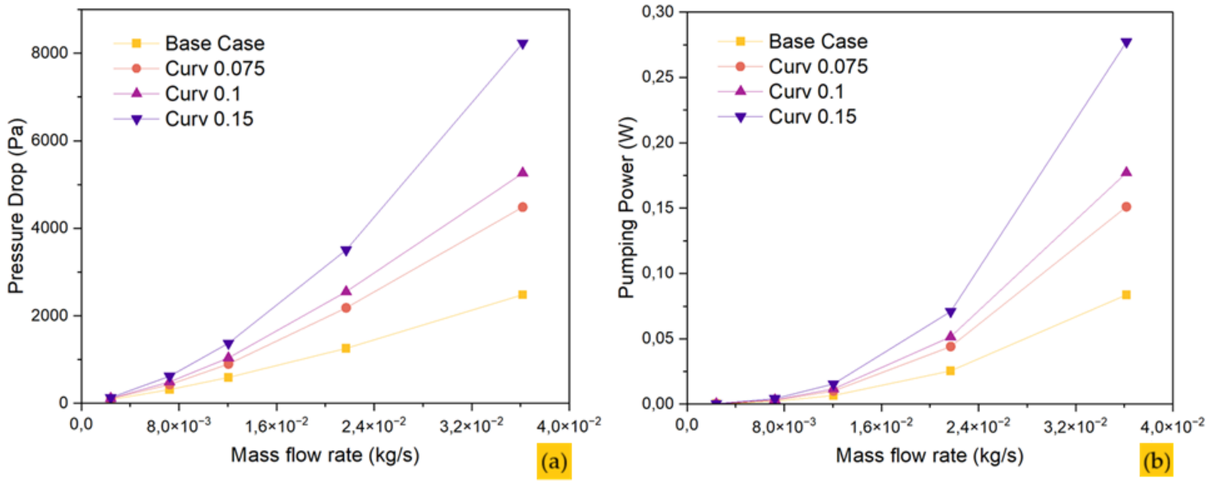

Figure 8. Curvature effect on: (a) Pressure drop; (b) Pumping power

dominant secondary flow compared to the primary flow in channels with sharper curvature [35].

Figure 9 shows the pressure distribution contour in a channel with low and high mass flow rates. A higher mass flow rate results in a greater pressure drop, consistent with Eq. (10) to Eq. (11). Furthermore, at the same mass flow rate, the pressure drop increases proportionally with the sharpness of the channel curvature. This phenomenon is attributed to the development of secondary flow induced by the channel curvature [52]. As illustrated in Figure 10, sharper curvatures generate stronger secondary flows within the channel.

The Cooling Efficiency Coefficient is shown in Figure 11a. This figure shows the effect of changes in mass flow rate on the cooling coefficient at several curvatures and C-rates. The highest Cooling Efficiency Coefficient occurs at C-rate 2, curvature 0.075 mm^{-1}, and mass flow rate 0.03618 kg/s. The lowest occurs at C-rate 0.5, curvature 0.15 mm^{-1}, and mass flow rate 0.03618 kg/s. Increasing the mass flow rate causes the Cooling Efficiency Coefficient to decrease. This indicates that increasing the flow requires a significant amount of flow energy. However, the energy removed through heat dissipation is still much larger than the pumping power. The baseline case gives the highest cooling efficiency coefficient for all C-rates. This is because the flow does not experience any losses caused by secondary flow. However, since the evaluation is based on steady-state data, the effect of curvature appears to be not very significant in this analysis. For the purpose of fast cooling, the benefit of using curvature can be better observed through a transient analysis.

Figure 11 (b) presents the Cooling Efficiency Coefficient as a function of Dean number for different curvature values and battery C-rates. An increase in Dean number leads to a decrease in the Cooling Efficiency Coefficient. This indicates that a higher Dean number strengthens the secondary flow, which raises the flow energy, and this increase in flow energy can reduce the cooling efficiency coefficient. Furthermore, at a 2 C rate,

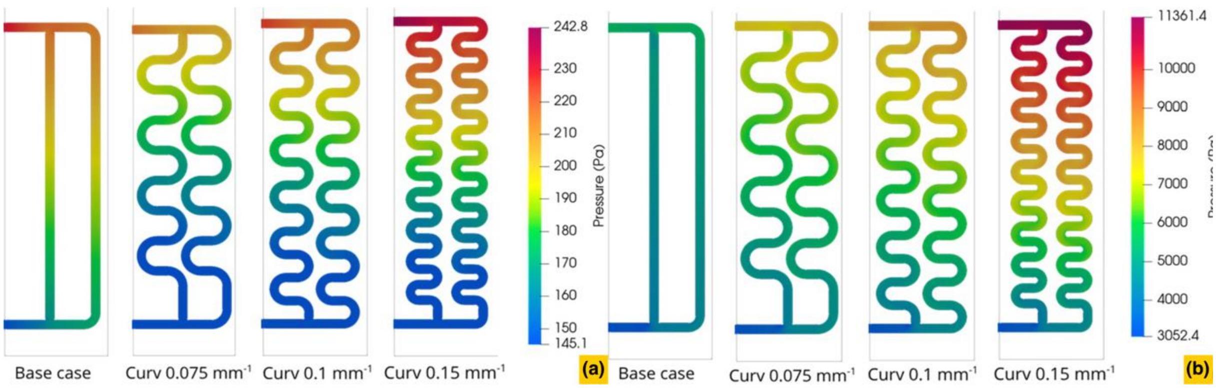

Figure 9. Pressure distribution of various cooling channels at mass flow rate: (a) 2.41×10^{-3} kg/s; (b) 3.61×10^{-2} kg/s

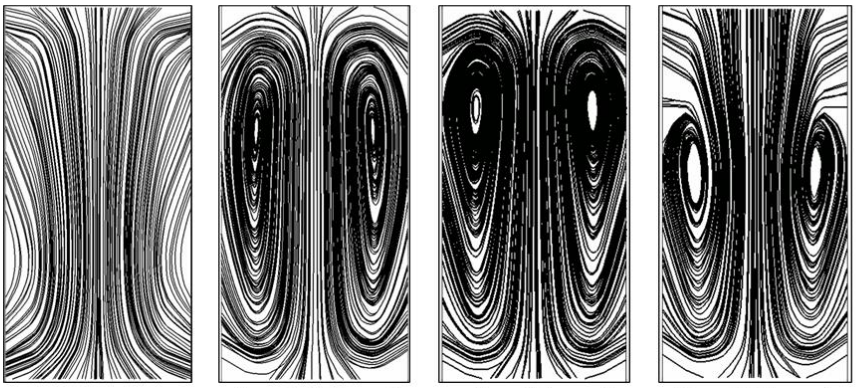

Figure 10. Streamline of various cooling channels

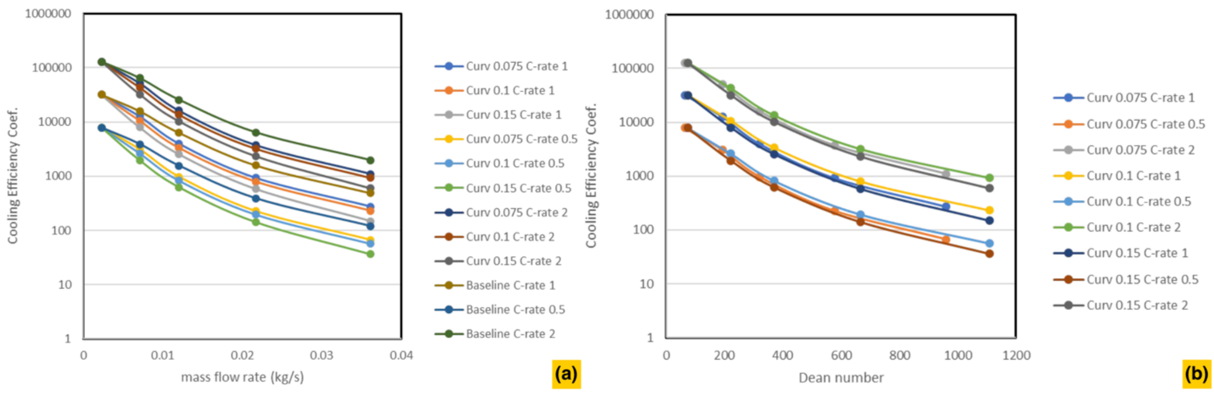

Figure 11. Cooling Efficiency Coefficient at various curvatures and C-rates: (a) At various mass flow rate; (b) At various Dean number

the Cooling Efficiency Coefficient is the highest across all curvatures and Dean numbers. This suggests that the energy transfer due to the heat dissipation rate is much more dominant than the energy carried by the flowing fluid.

Figure 12a shows the pressure drop per axial length of the channel. It can be seen that the pressure drop increases significantly as the mass flow rate increases. Furthermore, a larger curvature leads to a higher pressure drop per axial length. The pressure drop per axial length is not affected by the C-rate. On the other hand, the heat transfer rate per axial length increases with higher C-rate as seen in **Figure 12b**. Based on the heat dissipation rate results, it appears that curvature has no influence when using a steady-state approach. Therefore, in this figure, not only the effect of C-rate is observed.

3.4. *Transient Analysis*

A transient analysis was performed to observe several time dependent parameters such as $T_b max$, ΔT_b and heat dissipation rate (W). Same cooling design as steady case were simulated under three mass flow rates ($\dot{m}$=2.41 × 10⁻³ kg/s, 27.1 × 10⁻³ kg/s and 3.61 × 10⁻² kg/s) and three discharge rates (1C, 2C and 3C). All models were discharged up to 3600s. The result of this study is plotted in **Figure 13** and **Figure 14**.

Figure 13 depicts the $T_b max$ of cooling channels at different discharge rates and mass flow rates. As shown in **Figure 13**, the curves have similar trend with difference in $T_b max$ value based on their discharge rates. The results indicate that increasing the mass flow rate leads to a reduction in the $T_b max$ over the discharge period. Similar findings were reported by Sheng *et al*. [34] and Yang *et al*. [53] who also observed a decrease in the maximum temperature of the battery module with higher flow rates. This behaviour can be attributed to the balance between the heat generated by the battery pack and the heat removal capability of the coolant in the liquid cooling plate, as noted by Chen *et al*. [54].

In addition, the cooling channel with curvature performs better at higher mass flow rates, as indicated by the lower $T_b max$ compared to the base case cooling channel. However, at low mass

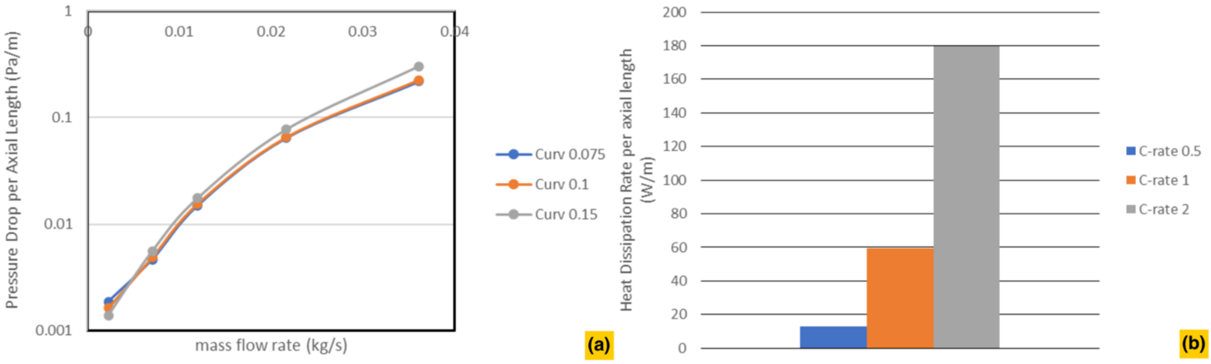

Figure 12. (a) Pressure drop per axial length; (b) Heat dissipation rate per axial length

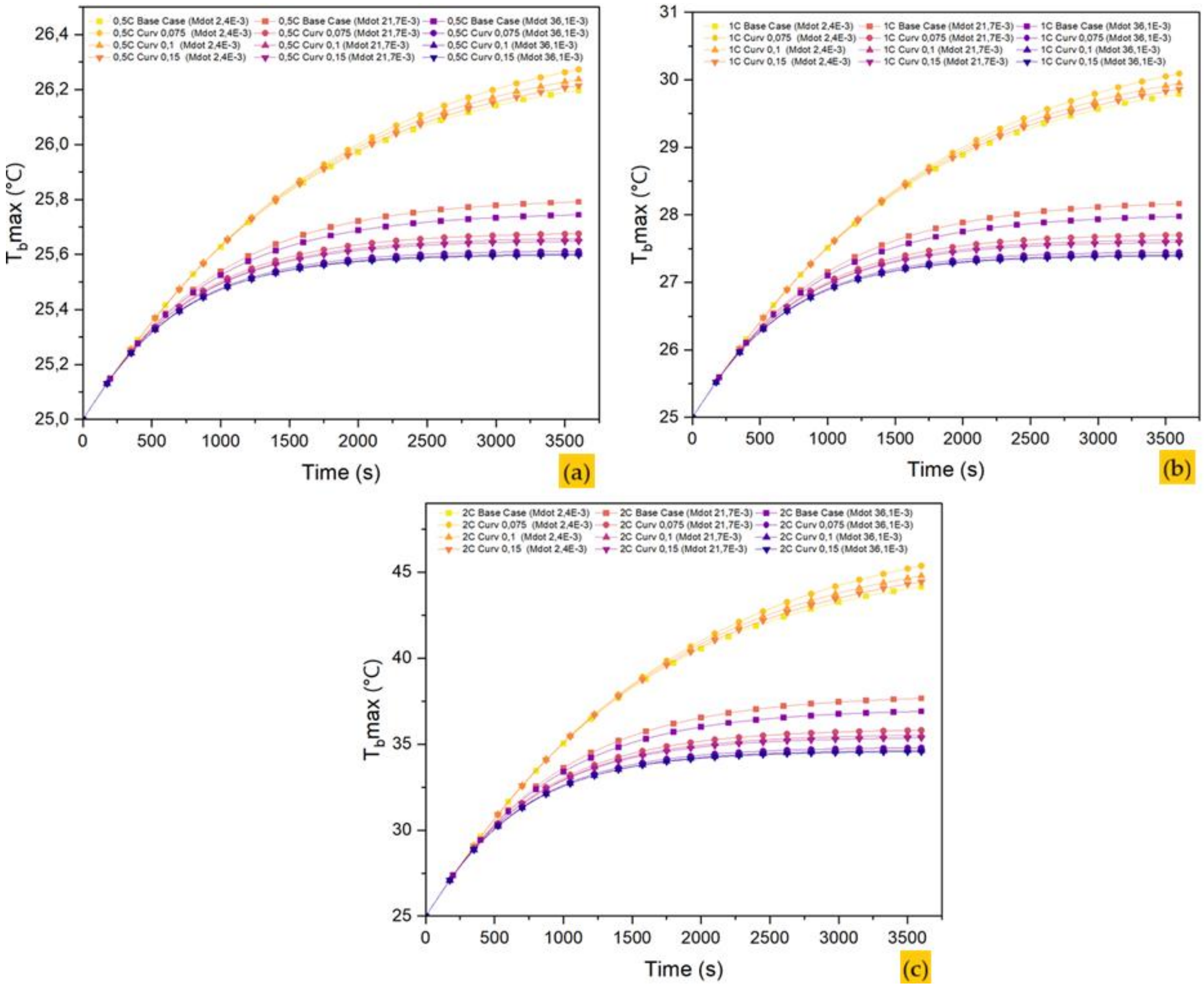

Figure 13. Battery maximum temperature at different discharge rates: (a) 1C; (b) 2C and (c) 3C

flow rates, curvature cooling channel exhibits a slightly higher $T_b max$ than the base case cooling channel. For example, at 1 C discharge rate and mass flow rate of 2.41×10⁻³ kg/s, the cooling channel with a curvature of 0.075 mm⁻¹ reaches a final $T_b max$ of 30.09 °C whereas the base case cooling channel reaches 29.78 °C. On the other hand, the curved cooling channels performs significantly better at higher mass flow rates. As an illustration, at a 1 C discharge rate with a mass flow rate of 3.61×10⁻² kg/s, the final $T_b max$ is 27.44 °C for the cooling channel with a curvature of 0.075 mm⁻¹ compared to 27.97 °C for the base-case channel. This difference may be due to the lower heat removal capability of curved cooling channels at low mass flow rate and their enhanced capability at high mass flow rates.

As mentioned in steady state section, another important aspect of BTMS is battery temperature difference (ΔT_b) which can be calculated by Eq.

(14). ΔT_b should not exceed 5 °C otherwise it would cause battery degradation and even thermal runaway [55]. **Figure 14** shows the relationship between coolant flow rate and ΔT_b, indicating that all discharge rates exhibit the same pattern. It shows that mass flow rate strongly influences ΔT_b as high mass flow rates consistently correspond to low ΔT_b values which is consistent with results found by Yates *et al.* [56]. For example, at 1C discharge rate, the cooling channel with a curvature of 0.1 mm^{-1} and a mass flow rate of 2.41 $\times$ 10^{-3} kg/s has a ΔT_b value of 3.20 °C. The same channel with mass flow rates of 27.1 $\times$ 10^{-3} kg/s and 36.1 $\times$ 10^{-3} kg/s has ΔT_b values of 2.12 °C and 2.07 °C respectively, representing reductions in ΔT_b of 40.16% and 42.88%.

Another finding is that cooling channels with low mass flow rates show lower ΔT_b than medium and high flow rates until about 1200 s, when the curves intersect. This occurs because at low mass flow rates, heat removal is slower, creating a temperature gradient between the centre batteries and those adjacent to the cooling plate as shown in **Figure 14**. A similar result was reported by Sheng *et al.* [34], where an intersection occurred at a specific time between the low and high mass flow rate curves. Another intersection between the medium and high mass flow rate curves appears at 1500 s. In addition, **Figure 15** shows that high mass flow rates quickly reach the battery heat generation rate, whereas low mass flow rates do not.

The battery heat generation model in this study employs a constant heat source. Under steady-state conditions, the results show that the heat dissipation rate remains constant as the mass flow rate increases as shown in **Figure 7**. However, the influence of curvature on the heat transfer rate is not negligible, as the time required for the three curvature configurations to reach steady state differs. To further investigate the effects of curvature and mass flow rate, a transient analysis was conducted for 0.5, 1 and 2 C discharge rates. The results of this analysis are presented in **Figure 13**.

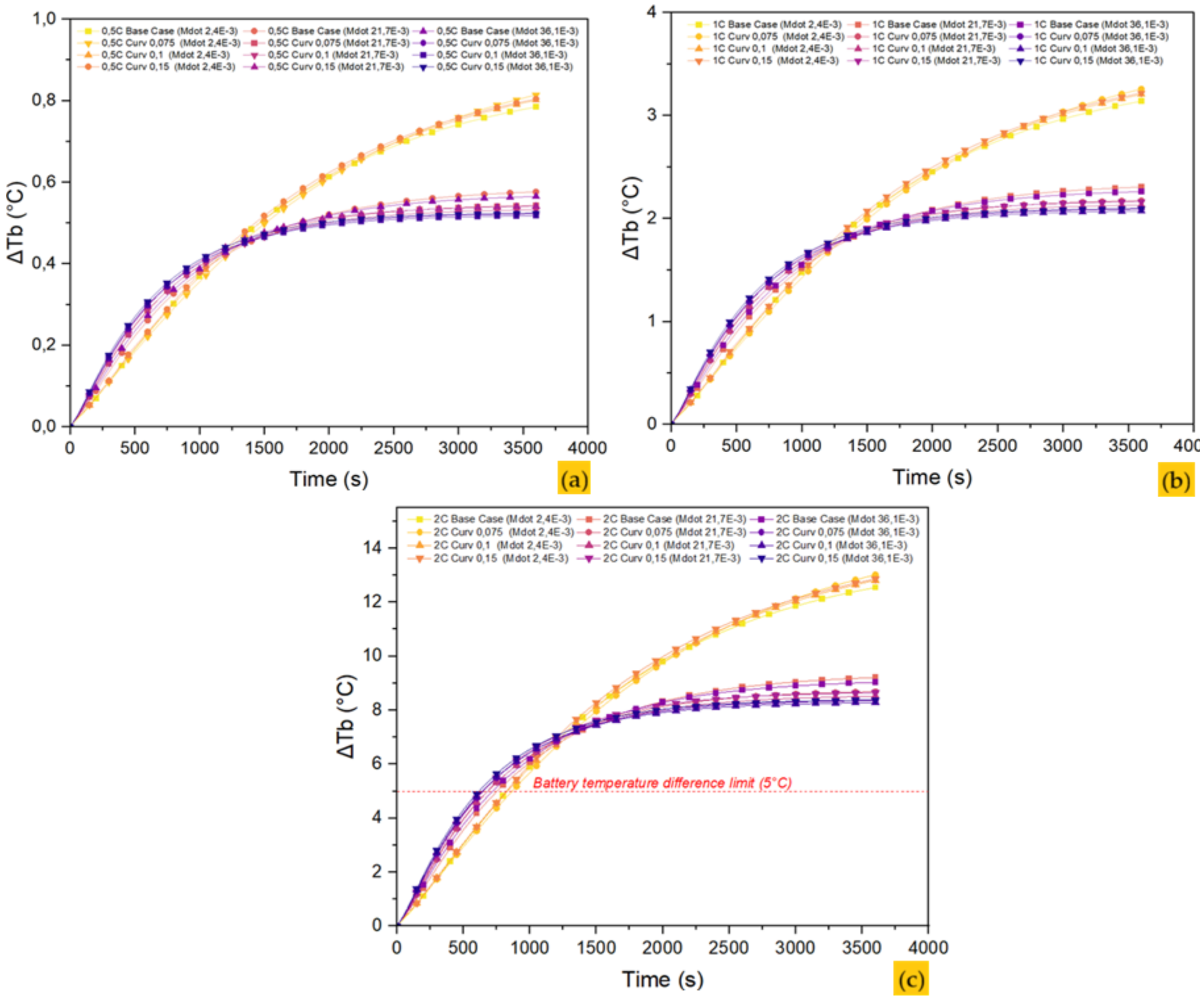

Figure 14. Battery temperature difference at different discharge rates: (a) 0.5C; (b) 1C and (c) 2C

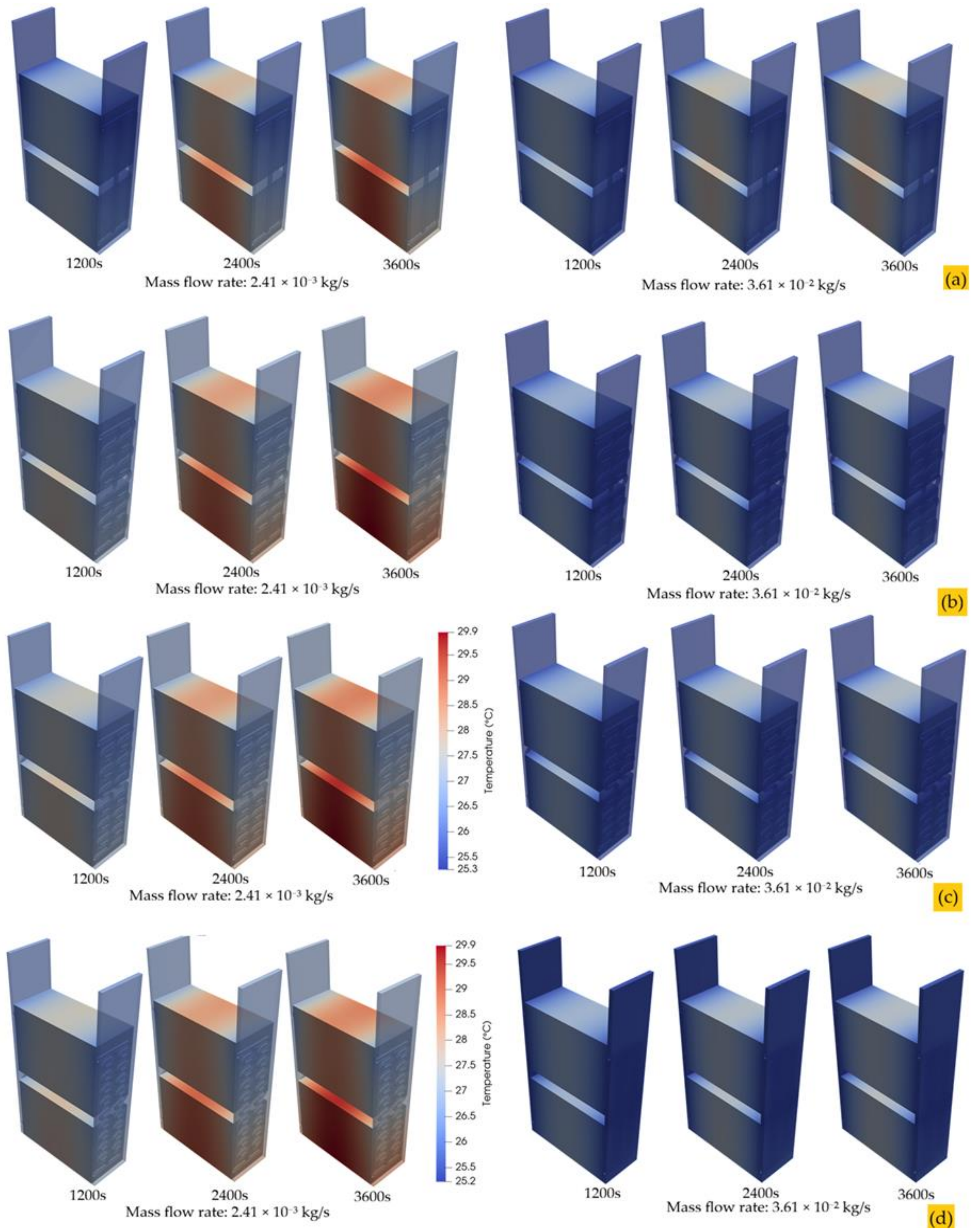

Figure 15. Battery temperature distribution at 1C discharge rate of different variations: (a) Base case, (b) Curv 0.075 mm^{-1}, (c) Curv 0.1 mm^{-1}, (d) Curv 0.15 mm^{-1}

As shown in **Figure 16**, all three discharge rates follow the same trend, differing only in their respective heat dissipation values. In general, cooling channels with low mass flow rates take longer to reach a steady state, where the heat removed equals to the heat generated by the battery. In contrast, medium and high mass flow rates achieve steady state much faster. This occurs because increasing the mass flow rate of the coolant improve the ability to remove heat from the battery by raising the convective heat transfer. Moreover, medium and high mass flow rates have similar values. This finding suggest that a medium flow rate could be a preferable choice

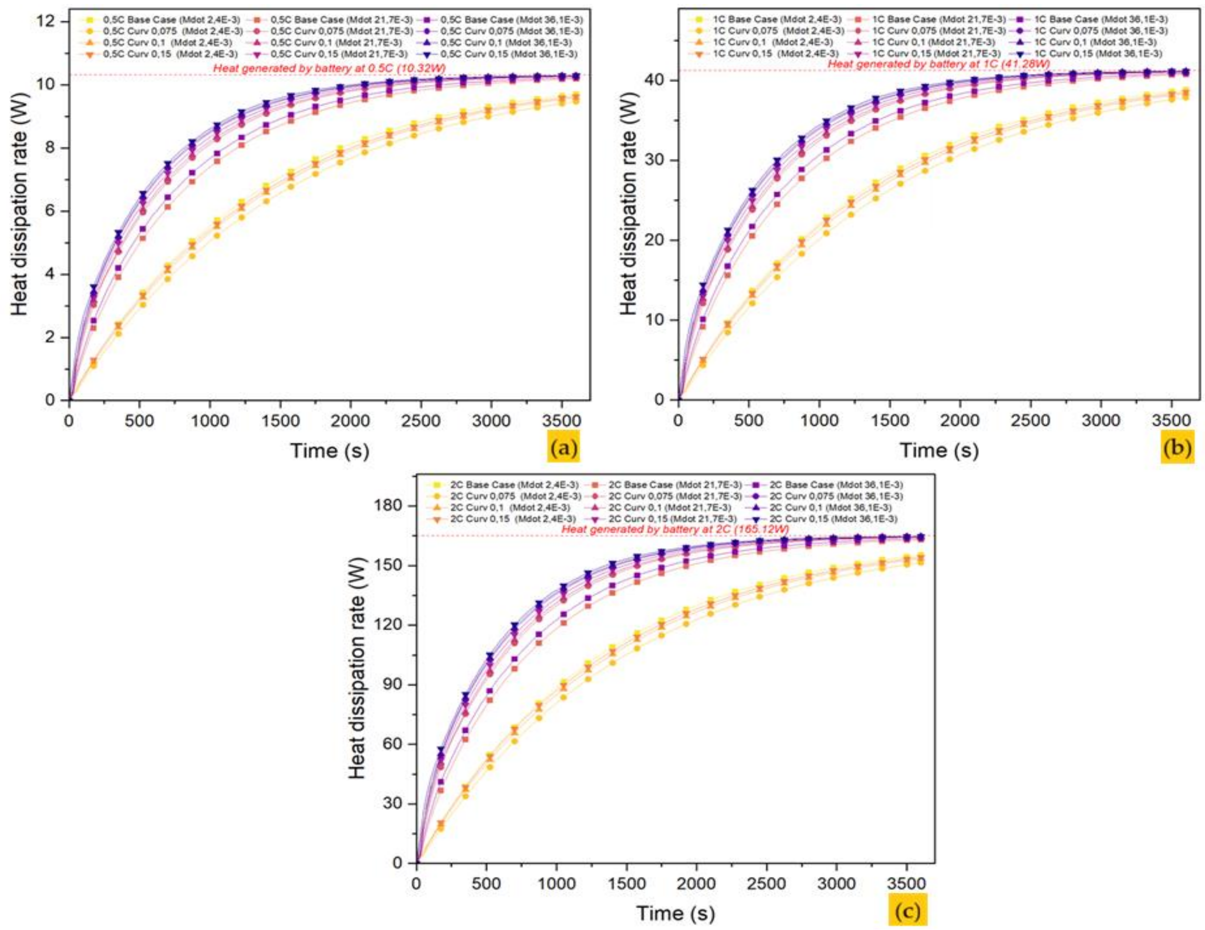

Figure 16. Heat dissipation rate at different discharge rates: (a) 1C; (b) 2C and (c) 3C

over a high flow rate due to the significant difference in pumping costs as shown in **Figure 8b**.

The curvature cooling channel exhibits better heat dissipation than the base-case cooling channel at medium and high mass flow rates during the early discharge period up to 1200 s (**Figure 16**). As discharge continues, these heat dissipation values converge. At mass flow rate of 36.1×10^{-3} kg/s and a discharge rate of 2C, the cooling channel curv 0.1 mm^{-1} achieves 144.35 W, compared to 132.50 W for the base case which is a difference of 8.56%. This high performance of curved cooling channel results from stronger secondary flow, which enhances local heat transfer and lowers both $T_b max$ and ΔT_b as shown in **Figure 13** and **Figure 14**. In contrast, at low mass flow rates, the base-case cooling channel maintains a slightly higher heat dissipation rate than the curvature cooling channel.

4. Conclusion

In summary, our findings confirm that increasing serpentine channel curvature reduces maximum battery temperature and improves temperature uniformity, but at the cost of higher pressure drop and pumping power. Among the three curvature values tested, 0.1 mm^{-1} offers the best trade-off. While the 0.15 mm^{-1} channel gives slightly better cooling, its pumping power (0.27 W at the highest flow rate) is nearly 60% higher than the base case, which is too large a penalty for the small thermal gain. The 0.075 mm^{-1} channel performs only marginally better than the base design. Therefore, 0.1 mm^{-1} is recommended as the optimal curvature for practical battery thermal management systems.

Regarding the 8.56% improvement in cooling performance (observed for the 0.1 mm^{-1} channel at 2C and 3.61×10^{-2} kg/s), we believe this gain is justified despite the increased pumping power. The absolute pumping power for all cases remains very low (below 0.3 W), so the extra energy cost is negligible compared to the benefit of keeping the battery within a safer and more uniform temperature range – especially during high-rate discharge where temperature differences can otherwise exceed 5 °C.

For real-world applications, a mass flow rate of around 1.21×10^{-2} kg/s is recommended. Higher flow rates produce only minor further reductions in maximum temperature, while lower flow rates (e.g., 2.41×10^{-3} kg/s) cause slower heat removal and larger temperature gradients. The medium flow rate also reaches thermal equilibrium almost as quickly as the highest flow rate, but with much less pumping power. In practice, for an electric bike battery pack, using a curvature of 0.1 mm^{-1} together with a flow rate of 1.21×10^{-2} kg/s provides a good balance between cooling effectiveness, temperature uniformity, and energy consumption.

Acknowledgements

We gratefully acknowledge the support provided by the Ministry of Higher Educations, Science, and Technology (KEMENDIKTISAINTEK) of Indonesia for the research on vocational education under national battery development consortium with contract: 134/SPK/D.D4/PPK.01.APTV/IV/2024 on April 29, 2024. This project would not have been possible without the funding and guidance under the Vocational Designation Program, which has played a critical role in advancing our study.

Author's Declaration

Authors' contributions and responsibilities

The authors made substantial contributions to the conception and design of the study. The authors took responsibility for data analysis, interpretation and discussion of results. The authors read and approved the final manuscript.

Funding

Ministry of Higher Educations, Science, and Technology (KEMENDIKTISAINTEK) of Indonesia under contract: 134/SPK/D.D4/PPK.01.APTV/IV/2024.

Availability of data and materials

All data are available from the authors.

Competing interests

The authors declare no competing interest.

Additional information

No additional information from the authors.

References

[1] J.-K. Kim, H. Park, S. Kim, J. Lee, Y. Song, and S. C. Yi, "Optimization models for the cost-effective design and operation of renewable-integrated energy systems," *Renewable and Sustainable Energy Reviews*, vol. 183, p. 113429, Sep. 2023, doi: 10.1016/j.rser.2023.113429.

[2] H. Lei, X. Hu, J. Zhao, D. Deng, and R. Wang, "Research Progress and Prospects of Public Transportation Charging Station Layout Methods," *World Electric Vehicle Journal*, vol. 15, no. 2, p. 63, Feb. 2024, doi: 10.3390/wevj15020063.

[3] Mohd Azri Abd Aziz *et al.*, "A Review on BLDC Motor Application in Electric Vehicle (EV) using Battery, Supercapacitor and Hybrid Energy Storage System: Efficiency and Future Prospects," *Journal of Advanced Research in Applied Sciences and Engineering Technology*, vol. 30, no. 2, pp. 41–59, Apr. 2023, doi: 10.37934/araset.30.2.4159.

[4] M. A. Fitrony, T. H. Ariwibowo, M. R. Rusli, E. H. Binugroho, and D. Pramadihanto, "A Thermal Investigation of Heat Sink with Dimple in Battery Cooling for Electric Motorbike Application," in *2024 International Electronics Symposium (IES)*, IEEE, Aug. 2024, pp. 1–6. doi: 10.1109/IES63037.2024.10665800.

[5] C. T. Yaw *et al.*, "Two phase heat transfer approaches for battery thermal management: Current status, challenges and future outlook," *Results in Engineering*, vol. 27, p. 105749, Sep. 2025, doi: 10.1016/j.rineng.2025.105749.

[6] M. S. Akhter, B. Moossa, R. Kahraman, S. Rasul, and R. A. Shakoor, "Advancements in high voltage, high-energy density, lithium-ion cathode materials: A focused review," *Applied Materials Today*, vol. 45, p. 102827, Aug. 2025, doi: 10.1016/j.apmt.2025.102827.

[7] S. Madaoui, J. Sabatier, J.-M. Vinassa, and F. Guillemard, "Research and implementation of a fast-charging methodology for lithium-ion batteries under bottom and dual cooling configurations," *Journal of Energy Storage*, vol. 130, p. 117285, Sep. 2025, doi: 10.1016/j.est.2025.117285.

[8] H. W. Xian, N. A. C. Sidik, and R. Saidur, "Hybrid nanocoolant for enhanced heat transfer performance in vehicle cooling system," *International Communications in Heat and Mass Transfer*, vol. 133, p. 105922, Apr. 2022, doi: 10.1016/j.icheatmasstransfer.2022.105922.

[9] N. A. C. Sidik, M. N. A. W. Muhamad, W. M. A. A. Japar, and Z. A. Rasid, "An overview of passive techniques for heat transfer augmentation in microchannel heat sink," *International Communications in Heat and Mass Transfer*, vol. 88, pp. 74–83, Nov. 2017, doi: 10.1016/j.icheatmasstransfer.2017.08.009.

[10] A. R. Abrari, T. H. Ariwibowo, D. Pramadihanto, N. R. Arini, and R. S. Dewanto, "Thermodynamic Analysis of Battery Thermal Management System in Electric Van for Tropical Climate: A Preliminary Study," in *2024 International Electronics Symposium (IES)*, IEEE, Aug. 2024, pp. 66–71. doi: 10.1109/IES63037.2024.10665770.

[11] C. Capasso, T. Castiglione, D. Perrone, and L. Sequino, "Thermal management of Li-ion batteries: Experimentally validated model of active temperature control strategies with liquid cooling and multi-objective optimization," *Journal of Energy Storage*, vol. 128, p. 117254, Aug. 2025, doi: 10.1016/j.est.2025.117254.

[12] Y. Ding, H. Ji, R. Liu, Y. Jiang, and M. Wei, "Study of the thermal behavior of a battery pack with a serpentine channel," *AIP Advances*, vol. 12, no. 5, May 2022, doi: 10.1063/5.0089378.

[13] J. S. Sakkera, R. Chintalapudi, B. Pappula, and S. Makgato, "Novel design of serpentine channel heat sinks with rectangular and triangular ribs and grooves for 25Ah Li-ion battery thermal management," *International Journal of Thermofluids*, vol. 25, p. 101011, Jan. 2025, doi: 10.1016/j.ijft.2024.101011.

[14] Y. Huo, Z. Rao, X. Liu, and J. Zhao, "Investigation of power battery thermal management by using mini-channel cold plate," *Energy Conversion and Management*, vol. 89, pp. 387–395, Jan. 2015, doi: 10.1016/j.enconman.2014.10.015.

[15] K. Monika, C. Chakraborty, S. Roy, S. Dinda, S. A. Singh, and S. P. Datta, "Parametric investigation to optimize the thermal management of pouch type lithium-ion batteries with mini-channel cold plates," *International Journal of Heat and Mass Transfer*, vol. 164, p. 120568, Jan. 2021, doi: 10.1016/j.ijheatmasstransfer.2020.120568.

[16] W. Dai and H. Lai, "Comparative study of flow-channel layout schemes in liquid cooling plates of a prismatic battery module," *Applied Thermal Engineering*, vol. 236, p. 121501, Jan. 2024, doi: 10.1016/j.applthermaleng.2023.121501.

[17] S. Hussen, R. K. Chanda, M. S. Alam, and R. N. Mondal, "Flow instability and development of dean vortices in a bending rectangular channel with bottom wall heating and cooling from the ceiling," *International Journal of Thermofluids*, vol. 26, p. 101049, Mar. 2025, doi: 10.1016/j.ijft.2024.101049.

[18] P. N. Shrirao, M. K. Chaudhary, and A. N. Patil, "Performance evaluation of heat transfer characteristics of heat exchanger in longitudinal fluid flow with serpentine tubes of constant pitch," *Materials Today: Proceedings*, vol. 72, pp. 864–869, 2023, doi: 10.1016/j.matpr.2022.09.082.

[19] D. Zhou, L. Qin, J. Yue, A. Yang, Z. Jiang, and S. Zheng, "Numerical and experimental investigations of spiral and serpentine micromixers over a wide Reynolds number range," *International Journal of Heat and Mass Transfer*, vol. 212, p. 124273, Sep. 2023, doi: 10.1016/j.ijheatmasstransfer.2023.124273.

[20] X. Hu *et al.*, "High-throughput separation of microplastic particles using a biomimetic filter in a serpentine microchannel," *Separation and Purification Technology*, vol. 376, p. 133841, Dec. 2025, doi: 10.1016/j.seppur.2025.133841.

[21] T. Ye, N. Phan-Thien, C. T. Lim, and Y. Li, "Red blood cell motion and deformation in a curved microvessel," *Journal of Biomechanics*, vol. 65, pp. 12–22, Dec. 2017, doi: 10.1016/j.jbiomech.2017.09.027.

[22] K. Monika and S. P. Datta, "Comparative assessment among several channel designs with constant volume for cooling of pouch-type battery module," *Energy Conversion and Management*, vol. 251, p. 114936, Jan. 2022, doi: 10.1016/j.enconman.2021.114936.

[23] L. Fan, J. Li, Y. Chen, D. Zhou, Z. Jiang, and J. Sun, "Study on the cooling performance of a new secondary flow serpentine liquid cooling plate used for lithium battery thermal management," *International Journal of Heat

and Mass Transfer, vol. 218, p. 124711, Jan. 2024, doi: 10.1016/j.ijheatmasstransfer.2023.124711.

[24] Z. Qian, Y. Li, and Z. Rao, "Thermal performance of lithium-ion battery thermal management system by using mini-channel cooling," *Energy Conversion and Management*, vol. 126, pp. 622–631, Oct. 2016, doi: 10.1016/j.enconman.2016.08.063.

[25] H. Najafi Khaboshan, F. Jaliliantabar, A. Adam Abdullah, and S. Panchal, "Improving the cooling performance of cylindrical lithium-ion battery using three passive methods in a battery thermal management system," *Applied Thermal Engineering*, vol. 227, p. 120320, Jun. 2023, doi: 10.1016/j.applthermaleng.2023.120320.

[26] M. Ignatowicz and B. Palm, "Experimental investigation of thermophysical properties of ethylene glycol based secondary fluids," *International Journal of Refrigeration*, vol. 155, pp. 137–153, Nov. 2023, doi: 10.1016/j.ijrefrig.2023.08.008.

[27] S. J. Bazinski, X. Wang, B. P. Sangeorzan, and L. Guessous, "Measuring and assessing the effective in-plane thermal conductivity of lithium iron phosphate pouch cells," *Energy*, vol. 114, pp. 1085–1092, Nov. 2016, doi: 10.1016/j.energy.2016.08.087.

[28] S. J. Bazinski and X. Wang, "Experimental study on the influence of temperature and state-of-charge on the thermophysical properties of an LFP pouch cell," *Journal of Power Sources*, vol. 293, pp. 283–291, Oct. 2015, doi: 10.1016/j.jpowsour.2015.05.084.

[29] L. Liang, Y. Zhao, Y. Diao, R. Ren, L. Zhang, and G. Wang, "Optimum cooling surface for prismatic lithium battery with metal shell based on anisotropic thermal conductivity and dimensions," *Journal of Power Sources*, vol. 506, p. 230182, Sep. 2021, doi: 10.1016/j.jpowsour.2021.230182.

[30] A. Mahmood, T. Cockerill, G. de Boer, J. Voss, and H. Thompson, "Heat Transfer Modeling and Optimal Thermal Management of Electric Vehicle Battery Systems," *Energies*, vol. 17, no. 18, p. 4575, Sep. 2024, doi: 10.3390/en17184575.

[31] T. Deng, G. Zhang, and Y. Ran, "Study on thermal management of rectangular Li-ion battery with serpentine-channel cold plate," *International Journal of Heat and Mass Transfer*, vol. 125, pp. 143–152, Oct. 2018, doi: 10.1016/j.ijheatmasstransfer.2018.04.065.

[32] Theodore L. Bergman, A. S. Lavine, F. P. Incropera, and D. P., *Fundamentals of Heat and Mass Transfer*, 8th ed. Wiley, 2017.

[33] J. Han, W. Ko, M.-S. Lim, T. Lee, and J. Yoo, "A numerical study of enhanced lithium-ion battery cooling using a module insert," *Case Studies in Thermal Engineering*, vol. 42, p. 102751, Feb. 2023, doi: 10.1016/j.csite.2023.102751.

[34] L. Sheng *et al.*, "Numerical investigation on a lithium ion battery thermal management utilizing a serpentine-channel liquid cooling plate exchanger," *International Journal of Heat and Mass Transfer*, vol. 141, pp. 658–668, Oct. 2019, doi: 10.1016/j.ijheatmasstransfer.2019.07.033.

[35] H. Choi, U. Han, and H. Lee, "Effects of diverging channel design cooling plate with oblique fins for battery thermal management," *International Journal of Heat and Mass Transfer*, vol. 200, p. 123485, Jan. 2023, doi: 10.1016/j.ijheatmasstransfer.2022.123485.

[36] A. Verma and D. Rakshit, "Performance analysis of PCM-fin combination for heat abatement of Li-ion battery pack in electric vehicles at high ambient temperature," *Thermal Science and Engineering Progress*, vol. 32, no. April, p. 101314, 2022, doi: 10.1016/j.tsep.2022.101314.

[37] X. Qian, D. Xuan, X. Zhao, and Z. Shi, "Heat dissipation optimization of lithium-ion battery pack based on neural networks," *Applied Thermal Engineering*, vol. 162, p. 114289, Nov. 2019, doi: 10.1016/j.applthermaleng.2019.114289.

[38] H. Behi *et al.*, "Thermal management analysis using heat pipe in the high current discharging of lithium-ion battery in electric vehicles," *Journal of Energy Storage*, vol. 32, p. 101893, Dec. 2020, doi: 10.1016/j.est.2020.101893.

[39] M. Shahjalal *et al.*, "A Numerical Thermal Analysis of a Battery Pack in an Electric Motorbike Application," *Designs*, vol. 6, no. 4, p. 60, Jun. 2022, doi: 10.3390/designs6040060.

[40] W. Shao *et al.*, "Study on the Reversible and Irreversible Heat Generation of the Lithium-Ion Battery with LiFePO4 Cathode," *Fire Technology*, vol. 59, no. 2, pp. 289–303, Mar. 2023, doi: 10.1007/s10694-022-01325-z.

[41] M.-K. Tran *et al.*, "A comprehensive equivalent circuit model for lithium-ion batteries, incorporating the effects of state of health, state of charge, and temperature on model parameters," *Journal of Energy Storage*, vol. 43, p. 103252, Nov. 2021, doi: 10.1016/j.est.2021.103252.

[42] W. Jung, H. K. Kim, M. Kim, and K.-J. Lee, "Spatial measurement of heat generation in a pouch-type lithium-ion battery," *International Journal of Precision Engineering and Manufacturing*, vol. 17, no. 8, pp. 1085–1089, Aug. 2016, doi: 10.1007/s12541-016-0132-7.

[43] A. R. Abrari, T. H. Ariwibowo, D. Pramadihanto, N. R. Arini, E. H. Binugroho, and A. Miyara, "Thermal Performance Enhancement of Serpentine Cooling Design Using Branch Modification for Lithium-Ion Batteries," *Automotive Experiences*, vol. 7, no. 3, pp. 552–566, Dec. 2024, doi: 10.31603/ae.12709.

[44] P. Naphon and J. Suwagrai, "Effect of curvature ratios on the heat transfer and flow developments in the horizontal spirally coiled tubes," *International Journal of Heat and Mass Transfer*, vol. 50, no. 3–4, pp. 444–451, Feb. 2007, doi: 10.1016/j.ijheatmasstransfer.2006.08.002.

[45] Y. Gan, L. He, J. Liang, M. Tan, T. Xiong, and Y. Li, "A numerical study on the performance of a thermal management system for a battery pack with cylindrical cells based on heat pipes," *Applied Thermal Engineering*, vol. 179, p. 115740, Oct. 2020, doi: 10.1016/j.applthermaleng.2020.115740.

[46] X. Fan *et al.*, "Numerical optimization of the cooling effect of a bionic fishbone channel liquid cooling plate for a large prismatic lithium-ion battery pack with high discharge rate," *Journal of Energy Storage*, vol. 72, p. 108239, Nov. 2023, doi: 10.1016/j.est.2023.108239.

[47] A. Vishwakarma and U. Rana, "Exploring serpentine cold-plate designs for efficient cooling of Li-ion pouch cells: A computational analysis," *International Journal of Heat and Mass Transfer*, vol. 244, p. 126896, Jul. 2025, doi: 10.1016/j.ijheatmasstransfer.2025.126896.

[48] Z. Tang, Z. Liu, J. Li, and J. Cheng, "A lightweight liquid cooling thermal management structure for prismatic batteries," *Journal of Energy Storage*, vol. 42, p. 103078, Oct. 2021, doi: 10.1016/j.est.2021.103078.

[49] S. Lin and L. Zhou, "Thermal performance of rectangular serpentine mini-channel cooling system on lithium battery," *Journal of Cleaner Production*, vol. 418, p. 138125, Sep. 2023, doi: 10.1016/j.jclepro.2023.138125.

[50] P. Ni and X. Wang, "Temperature field and temperature difference of a battery package for a hybrid car," *Case Studies in Thermal Engineering*, vol. 20, p. 100646, Aug. 2020, doi: 10.1016/j.csite.2020.100646.

[51] H. Jouhara *et al.*, "Applications and thermal management of rechargeable batteries for industrial applications," *Energy*, vol. 170, pp. 849–861, Mar. 2019, doi: 10.1016/j.energy.2018.12.218.

[52] W. M. Abed, R. D. Whalley, D. J. C. Dennis, and R. J. Poole, "Numerical and experimental investigation of heat transfer and fluid flow characteristics in a micro-scale serpentine channel," *International Journal of Heat and Mass Transfer*, vol. 88, pp. 790–802, Sep. 2015, doi: 10.1016/j.ijheatmasstransfer.2015.04.062.

[53] H. Yang, N. Liu, M. Gu, Q. Gao, and G. Yang, "Optimized design of novel serpentine channel liquid cooling plate structure for lithium-ion battery based on discrete continuous variables," *Applied Thermal Engineering*, vol. 264, p. 125502, Apr. 2025, doi: 10.1016/j.applthermaleng.2025.125502.

[54] C. Chen, Y. Qian, G. Xu, Q. Zhang, and P. Lu, "Numerical investigation on thermal management performance of soft packing Li-ion batteries with oblique multi-channel cold plates," *Renewable Energy*, vol. 234, p. 121250, Nov. 2024, doi: 10.1016/j.renene.2024.121250.

[55] L. Wang, H. Zuo, B. Zhang, and G. Jia, "Effects of the cold plate with airfoil fins on the cooling performance enhancement of the prismatic LiFePO4 battery pack," *Energy*, vol.

296, p. 131210, Jun. 2024, doi: 10.1016/j.energy.2024.131210.

[56] M. Yates, M. Akrami, and A. A. Javadi, "Analysing the performance of liquid cooling designs in cylindrical lithium-ion batteries," *Journal of Energy Storage*, vol. 33, p. 100913, Jan. 2021, doi: 10.1016/j.est.2019.100913.